JNS 1 (2012) 27-38

Journal of
NANOSTRUCTURES
JNS
NANOSTRUCTURES
JNS.kashanu.ac.ir

Thermo-elastic behavior of a thick-walled composite cylinder reinforced with functionally graded SWCNTs

A. Ghorbanpour-Arani[a, b, *], V. Sadooghi[a], M. R. Mozdianfard[c], M. Mohammadimehr[a]

[a] *Department of Mechanical Engineering, Faculty of Engineering, University of Kashan, Kashan, I. R. Iran*

[b] *Institute of Nanoscience & Nanotechnology, University of Kashan, Kashan, I.R.Iran.*

[c] *Department of Chemical Engineering, Faculty of Engineering, University of Kashan, Kashan, I. R. Iran.*

Article history:
Received 1/9/2011
Accepted 16/12/2011
Published online 1/1/2012

Keywords:
Stress analysis
Reinforced FG SWCNTs
Composite
Thick-walled cylinder

**Corresponding author:*
E-mail address:
aghorban@kashanu.ac.ir
Phone: +98 9131626594
Fax: +98 361 5513011

Abstract

In this article, thermo-elastic-behavior of a thick-walled cylinder made from a polystyrene nanocomposite reinforced with functionally graded (FG) single-walled carbon nanotubes (SWCNTs) was carried out in radial direction while subjected to a steady state thermal field. The SWCNTs were assumed aligned, straight with infinite length and a uniform layout. Two types of variations in the volume fraction of SWCNTs were considered in the structure of the FG cylinder along the radius from inner to outer surface, namely: incrementally increasing (Inc Inc) and incrementally decreasing (Inc Dec). These are compared with uniformly distributed (UD) structure. Mori-Tanaka method was used for stress-strain analysis. Using equations of motion, stress-strain and their corresponding constitutive correlations of a polystyrene vessel, a second order ordinary differential equation was proposed based on the radial displacement which was solved in order to obtain the distribution of displacement and radial, circumferential and axial stresses. For constant temperatures at the inner and outer surfaces of the FG cylinder considered here, results in this work indicate that radial and circumferential stresses and displacement are lower for the Inc Inc FG cylinder, and the axial stresses are higher irrespective of the structure of the FG material.

1. Introduction

Following the discovery of carbon nanotubes (CNTs) by Iijima in 1990's, and considering their extremely high Young modulus of 1 TPa in axial direction for both single and multi-walled carbon

nanotubes (SWCNTs & MWCNTs), there has been ever increasing interests on their mechanical, thermal and electrical characteristics [1-2]. CNTs with high strength and low density have been considered as appropriate fillers in polymer composites, and properties such as dispersion, buckling and collapse of embedded CNTs in the matrix as well as the interfacial bonding between CNTs and matrix have received great attentions by many workers [3-7].

Considering nanocomposite applications in actual structures, Qian et al. [8] reported a MWCNTs reinforced by polystyrene with good dispersion and CNT-matrix adhesion. They achieved improvements of 40% in the elastic modulus and 25% in the tensile strength by adding only 0.5% CNT. Odergart et al. [9] presented techniques to evaluate elastic properties of nanocomposites and found that adding volume fraction by 1% yielded a maximum stiffness for CNT length of 60-80 nm for both aligned and random orientations. Wuite and Adali [10] examined deflection and stress of nanocomposite reinforced beams and reported significant improvement in beam stiffness. Bending and local buckling of a nanocomposite beam reinforced by a SWCNT was also studied by Vodenitcharova and Zhang [11]. Studies conducted by Han and Elliot [12] and Zhu et al. [13] on simulation of the elastic properties of polymer/CNT composites and stress-strain curves for CNT reinforced Epon 862 composites, respectively, suggested that addition of a small amount of CNT improved mechanical, electrical and thermal properties of polymeric composites. Their useful results can be applied to the global response of CNT reinforced with composites in an actual structural element.

Functionally graded materials (FGMs) are a new generation of composites in which the micro-structural details are spatially varied through non-uniform distribution of the reinforcement phase in order to improve properties such as linear and nonlinear bending behaviors, and interfacial bonding strength. Shen [14] studied these for the plates at various thermal environments; while Ke et al. [15] examined nonlinear free-vibration of FGM carbon nanotube reinforced composites for beams. As far as work on cylinder is concerned which extensive workers have been carried out due to industrial interests hallow cylinders for analysis of thermally excited responses to elastic bodies [16-17]. Ding et al. [18] studied a theoretical solution of cylindrically isotropic cylindrical tube for the axisymmetric plane strain dynamic thermoelastic problem. For pyroelectric material, Pelletier and Vel [19] presented an exact solution for the steady-state thermoelastic response of functionally graded orthotropic cylindrical shells. As for non-homogeneity of materials, the special case where the Young's modulus has a power law dependence on the radial coordinate, with the linear thermal expansion coefficient and the constant Poisson's ratio has been studied by many workers [20-21]. Abd-Alla and Farhan [22] analyzed the effect of the non-homogenity on the composite infinite cylinder of orthotropic material.

In this present work, the concept of functionally graded material is applied to the nanocomposite cylinder reinforced by SWCNTs. Material properties of SWCNTs are assumed to be temperature dependent. The material properties of functionally graded CNTRCs are assumed to be graded in radial direction. The cylinder is subjected to a steady state thermal field. The Mori-Tanaka method is used for stress-strain analysis. Using equations of motion, stress-strain and their corresponding constitutive correlations of a polystyrene vessel, a second order ordinary

differential equation is proposed based on the radial displacement which is solved in order to obtain the distribution of radial, circumferential and axial stresses.

2. Governing equations

In this study, Mori-Tanaka method was used to determine the effective material properties of the SWCNTs reinforced by polystyrene nanocomposite due to its simplicity and accuracy at high volume fraction of CNTs inclusions [23]. Similar to [23] a representative volume element (RVE) V for the composite is illustrated in Fig. 1, in which a linear elastic polymer matrix is reinforced by a SWCNT that is aligned, straight and infinite in length in x2 direction.

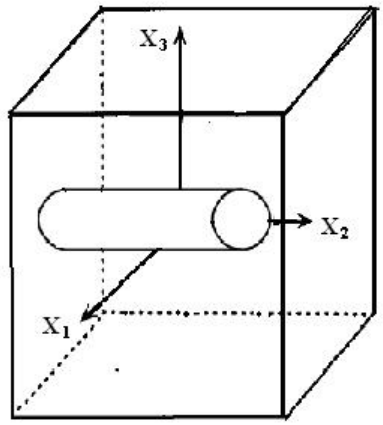

Fig. 1. A representative element of a composite reinforced with aligned straight CNTs.

The RVE boundary of δV is also subjected either to tractions corresponding to a uniform overall stress σ0 or to displacements compatible to a prescribed uniform overall strain ε0 and the method assumes that each inclusion is embedded in an infinite pristine matrix subjected to an effective average stress σm or an effective average strain εm in the far field [8]. The matrix is also assumed to be elastic and isotropic. Each straight CNT is modeled as a long fiber with transversely isotropic elastic properties. Therefore, the composite too, is transversely isotropic; its constitutive relation $\sigma = C : \varepsilon$ can be expressed as [23]:

$$\begin{Bmatrix} \sigma_{11} \\ \sigma_{22} \\ \sigma_{33} \\ \sigma_{23} \\ \sigma_{13} \\ \sigma_{12} \end{Bmatrix} = \begin{bmatrix} k+m & l & k-m & 0 & 0 & 0 \\ l & n & l & 0 & 0 & 0 \\ k-m & l & k+m & 0 & 0 & 0 \\ 0 & 0 & 0 & p & 0 & 0 \\ 0 & 0 & 0 & 0 & m & 0 \\ 0 & 0 & 0 & 0 & 0 & p \end{bmatrix} \begin{Bmatrix} \varepsilon_{11} \\ \varepsilon_{22} \\ \varepsilon_{33} \\ \varepsilon_{23} \\ \varepsilon_{13} \\ \varepsilon_{12} \end{Bmatrix} \quad (1)$$

where k, l, m, n, and p are Hill's elastic moduli; k is the plane-strain bulk modulus normal to the fiber direction, n is the uniaxial tension modulus in the fiber direction (x_2), l is the associated cross modulus, m and p are the shear moduli in planes normal and parallel to the fiber direction, respectively. These are expressed mathematically as follows [24]:

$$k = \frac{E_m\{E_m c_m + 2k_r(1+\nu_m)[1+c_r(1-2\nu_m)]\}}{2(1+\nu_m)[E_m(1+c_r-2\nu_m)+2c_m k_r(1-\nu_m-2\nu_m^{\,2})]} \quad (2a)$$

$$l = \frac{E_m\{c_m\nu_m[E_m+2k_r(1+\nu_m)]+2c_r l_r(1-\nu_m^{\,2})\}}{(1+\nu_m)[2c_m k_r(1-\nu_m-2\nu_m^{\,2})+E_m(1+c_r-2\nu_m)]} \quad (2b)$$

$$n = \frac{E_m^{\,2} c_m(1+c_r-c_m\nu_m)+c_m c_r(k_r n_r - l_r^{\,2})(1+\nu_m)^2(1-2\nu_m)}{(1+\nu_m)\{2c_m k_r(1-\nu_m-2\nu_m^{\,2})+E_m(1+c_r-2\nu_m)\}} + \frac{E_m[2c_m^{\,2}k_r(1-\nu_m)+c_r n_r(1-2\nu_m+c_r)-4c_m l_r\nu_m)]}{2c_m k_r(1-\nu_m-2\nu_m^{\,2})+E_m(1-2\nu_m+c_r)} \quad (2c)$$

$$p = \frac{E_m[E_m c_m + 2(1+c_r)p_r(1+\nu_m)]}{2(1+\nu_m)[E_m(1+c_r)+2c_m p_r(1+\nu_m)]} \quad (2d)$$

$$m=\frac{E_m[E_m c_m+2m_r(1+\nu_m)(3+c_r-4\nu_m)]}{2(1+\nu_m)\{E_m[c_m+4c_r(1-\nu_m)]+2c_m m_r(3-\nu_m-\nu_m^{\,2})\}} \quad (2e)$$

Where E_m and υ_m are Young's modulus and Poisson's ratio, respectively, and k_r, l_r, m_r, n_r and p_r are the Hill's elastic moduli for the reinforcing phase (CNTs). For polystyrene $E_m = 1.9\,Gpa$ and $\upsilon_m = 0.3$ and Hill's elastic moduli of SWCNTs with 10 A° and 20 A° radii are listed in Table 1 [23, 25].

Table 1. Hill's elastic moduli of reinforced CNTs.

CNT Radius (A°)	k_r (Gpa)	l_r (Gpa)	m_r (Gpa)	n_r (Gpa)	p_r (Gpa)
10	30	10	1	450	1
20	4	2	0.1	250	0.1

2.1. Thermal analysis

Consider a thick-walled FG polystyrene nanocomposite cylinder with infinite length as illustrated in Fig. 2. Straight SWCNTs are embedded along the axial direction of the cylinder.

Assuming cylindrical coordinate system (r, θ, z), and the volume fraction of the constituent (c) for both the reinforced CNT material and the matrix are cr and cm, then [14]:

$$c_r + c_m = 1 \quad (3)$$

As can be seen from Fig. 3a, when the volume fraction of SWCNTs is uniformly distributed (UD), cr is defined as follow:

$$c_r = V_{CN}^{\,*} \quad (4)$$

where

$$V_{CN}^{\,*} = \frac{w_{CN}}{w_{CN} + (\rho_{CN}/\rho_m) - (\rho_{CN}/\rho_m) w_{CN}}$$

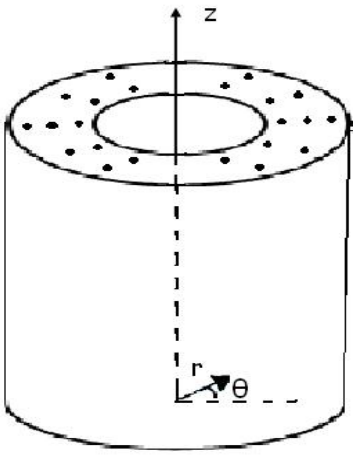

Fig.2. A thick-walled nanocomposite cylinder embedded with straight SWCNTs along the axial direction.

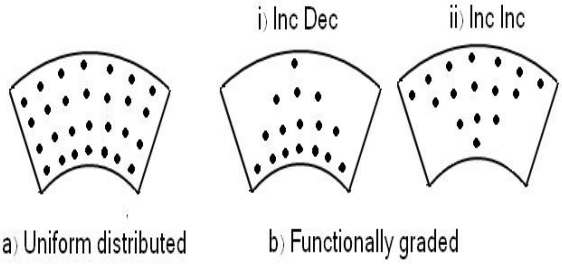

Fig. 3. Variations in the volume fraction of SWCNTs considered a) uniformly distributed and b) functionally graded i) Inc Dec, and ii) Inc-Inc

And wCN is the mass fraction of the SWCNTs, ρm and ρCN are densities of matrix and carbon nanotubes, respectively, and VCN* specific volume fraction of carbon nanotube. With respect to FG material, two types of variations (or layouts) in the volume fraction of SWCNTs were considered in the structure of the FG cylinder along the radius from inner to outer surface, namely: incrementally decreasing (Inc Dec) and incrementally increasing (Inc Inc). (see Fig. 3b). The former refers to the structure in which the volume fraction of the SWCNTs is reduced from

inner to outer surface, while for the latter, this is increased cr for both Inc Dec and Inc Inc are as explained below in Eqs. 5 and 6, respectively:

$$c_r = (1+2\frac{1-\zeta}{1-h})V_{CN}^{*} \quad (5)$$

$$c_r = (1+2\frac{\zeta-h}{1-h})V_{CN}^{*} \quad (6)$$

Where ζ and h are the dimensionless radius and ratio of the inner to outer radius of the cylinder or aspect ratios, respectively, i.e.

$$\zeta = \frac{r}{r_o} \quad , \quad h = \frac{r_i}{r_o} \quad (7)$$

The physical properties for polystyrene and SWCNTs are as follows [14, 26]:

$$\rho_m = 1.05(kg/m^3), \qquad \rho_{CN} = 1.4(kg/m^3)$$

$$w_{CN} = 0.13, \qquad V_{CN}^{*} = 0.11$$

The general equations of motion and strain-displacement relations for a thick-walled cylinder could be written as [18]:

$$\frac{\partial\sigma_{rr}}{\partial r}+\frac{1}{r}\frac{\partial\sigma_{r\theta}}{\partial\theta}+\frac{\partial\sigma_{rz}}{\partial z}+\frac{\sigma_{rr}-\sigma_{\theta\theta}}{r}+F_r=\rho\frac{\partial^2 u_r}{\partial t^2}$$

$$\frac{\partial\sigma_{\theta r}}{\partial r}+\frac{1}{r}\frac{\partial\sigma_{\theta\theta}}{\partial\theta}+\frac{\partial\sigma_{\theta z}}{\partial z}+\frac{2\sigma_{\theta r}}{r}+F_\theta=\rho\frac{\partial^2 u_\theta}{\partial t^2}$$

$$\frac{\partial\sigma_{zr}}{\partial r}+\frac{1}{r}\frac{\partial\sigma_{z\theta}}{\partial\theta}+\frac{\partial\sigma_{zz}}{\partial z}+\frac{\sigma_{zr}}{r}+F_z=\rho\frac{\partial^2 u_z}{\partial t^2} \quad (8)$$

$$\varepsilon_{rr}=\frac{\partial u_r}{\partial r}, \qquad \varepsilon_{r\theta}=\frac{1}{2}(\frac{\partial u_\theta}{\partial r}+\frac{1}{r}\frac{\partial u_r}{\partial\theta}-\frac{u_\theta}{r})$$

$$\varepsilon_{\theta\theta}=\frac{1}{r}\frac{\partial u_\theta}{\partial\theta}+\frac{u_r}{r}, \qquad \varepsilon_{\theta z}=\frac{1}{2}(\frac{\partial u_\theta}{\partial z}+\frac{1}{r}\frac{\partial u_z}{\partial\theta})$$

$$\varepsilon_{zz}=\frac{\partial u_z}{\partial z}, \qquad \varepsilon_{rz}=\frac{1}{2}(\frac{\partial u_z}{\partial r}+\frac{\partial u_r}{\partial z}) \quad (9)$$

When the nanocomposite cylinder is subjected to a thermal field, thermal strains are created in three directions in the stress-strain relations as in Eq. (10) as follows [18]:

$$\begin{Bmatrix}\sigma_r\\ \sigma_z\\ \sigma_\theta\\ \sigma_{\theta z}\\ \sigma_{zr}\\ \sigma_{r\theta}\end{Bmatrix}=\begin{bmatrix}k+m & l & k-m & 0 & 0 & 0\\ l & n & l & 0 & 0 & 0\\ k-m & l & k+m & 0 & 0 & 0\\ 0 & 0 & 0 & p & 0 & 0\\ 0 & 0 & 0 & 0 & m & 0\\ 0 & 0 & 0 & 0 & 0 & p\end{bmatrix}\begin{Bmatrix}\varepsilon_r-\lambda_r T\\ \varepsilon_z-\lambda_z T\\ \varepsilon_\theta-\lambda_\theta T\\ 2\gamma_{\theta z}\\ 2\gamma_{zr}\\ 2\gamma_{r\theta}\end{Bmatrix} \quad (10)$$

Where λ is the thermal modulus, T denotes the temperature expressed in absolute unit. In Eq. (10), elastic modulus and thermal expansion coefficients are related as follows [18]:

$$\begin{cases}\lambda_r=C_{11}\alpha_r+C_{12}\alpha_z+C_{13}\alpha_\theta\\ \lambda_z=C_{21}\alpha_r+C_{22}\alpha_z+C_{23}\alpha_\theta\\ \lambda_\theta=C_{31}\alpha_r+C_{32}\alpha_z+C_{33}\alpha_\theta\end{cases}$$

$$\begin{cases}C_{11}=k+m\\ C_{12}=l\\ C_{11}=k-m\end{cases} \quad (11)$$

Based on Mori-Tanaka method, nanocomposite characteristics are assumed to be transversely isotropic which can only be applied where SWCNTs are uniformly distributed. This is because the nanocomposite characteristics are orthotropic for FG materials. Despite this, assuming the structure is almost uniform and cr changes slightly and linearly in such a way that properties do not alter significantly in radial and circumferential directions, one might employ the introduced stiffness matrix in Eq. (1) for FG materials.

The thermal expansion coefficients of nanocomposite in z, r and θ directions may be written as:

$$\alpha_z = c_r \alpha_z^{CN} + c_m \alpha^m \quad (12a)$$

$$\alpha_r = (1+\nu_z^{CN}) c_r \alpha_r^{CN} + (1+\nu^m) c_m \alpha^m - \nu_\zeta \times \alpha_z \quad (12b)$$

$$\alpha_r = \alpha_\theta \quad (12c)$$

$$\nu_\zeta = c_r \nu_z^{CN} + c_m \nu^m \quad (13)$$

Where $\alpha_r^{CN}, \alpha_z^{CN}$ are thermal expansion coefficients of SWCNTs in longitudinal and radial directions, respectively, and α^m is the thermal expansion coefficient of the matrix assumed to be $\alpha^m = 7\times10^{-5}(K^{-1})$ [26].

Table 2. Temperature-dependent thermal expansion coefficients of SWCNTs in the longitudinal and radial directions [14].

Temperature (K)	α_Z^{CN} $(\times10^{-6}/K)$	α_r^{CN} $(\times10^{-6}/K)$
300	3.4584	5.1682
500	4.5361	5.0189
700	4.6677	4.8943

However, $\alpha_r^{CN}, \alpha_z^{CN}$ are not expected to alter significantly for the temperature range of 300K<T<700K considered in this work. Hence, their average values are taken at 500K from the data used by [14] as expressed in Table 2. Also, in the above equations, $\upsilon_z^{CN}, \upsilon_m$ are Poisson's ratios SWCNTs and matrix assumed to be $\upsilon_z^{CN} = 0.175$, $\upsilon_m = 0.3$ [14, 23].

For practical purposes, stress, strain and thermal moduli can be rewritten in dimensionless form of as follows:

$$\theta = \frac{T}{T_0} \qquad \varepsilon_\theta = \alpha_r T_0 \frac{u_0}{\zeta} \qquad \varepsilon_r = \alpha_r T_0 \frac{\partial u_0}{\partial \zeta}$$

$$u_0 = \frac{u}{\alpha_r T_0 b} \qquad \Lambda_i = \frac{\lambda_{ii}}{C_{11}\alpha_r} \quad (i = r,z,\theta)$$

$$\sigma_i = \frac{\sigma_{ii}}{\alpha_r T_0 C_{11}} \quad (i = r,z,\theta) \quad (14)$$

$$u_0'' + \frac{u_0'}{\zeta} - \frac{u_0}{\zeta^2} - \left(\frac{\partial \Lambda_r}{\partial \zeta}\theta + \Lambda_r \frac{\partial \theta}{\partial \zeta}\right) = 0 \quad (15)$$

The boundary conditions are defined as:

$$\sigma_r(h) = 0 \qquad \sigma_r(1) = 0 \quad (16)$$

In order to solve Eq. (16), the temperature distribution should be determined. The general form of the governing equation of heat conduction in cylindrical coordinates can be written as [27]:

$$k\left(\frac{\partial^2 T}{\partial r^2} + \frac{1}{r}\frac{\partial T}{\partial r} + \frac{1}{r^2}\frac{\partial^2 T}{\partial \phi^2} + \frac{\partial^2 T}{\partial z^2}\right) + R = \rho c \frac{\partial T}{\partial t} \quad (17)$$

Where k, R, and c are conductivity, rate of heat generation and specific thermal capacity, respectively. Assuming infinite length for the cylinder, no internal heat generation, steady state thermal field and axisymmetrical temperature distribution (i.e. $\frac{\partial^2 T}{\partial \phi^2} = 0$, $\frac{\partial^2 T}{\partial z^2} = 0$), the heat transfer equation is simplified to:

$$\left(\frac{\partial^2 T}{\partial r^2} + \frac{1}{r}\frac{\partial T}{\partial r}\right) = 0 \quad (18)$$

For dimensionless form, Eq. (18) is expressed as:

$$(\frac{\partial^2\theta}{\partial\zeta^2}+\frac{1}{\zeta}\frac{\partial\theta}{\partial\zeta})=0 \quad (19)$$

Assuming temperature at both inner and outer surfaces of the cylinder remains constant as Ti=300K and To=500K, respectively, with the surrounding temperature of T0=300K, the temperature profile is written in the following form:

$$\theta = A + B\ln\zeta \quad (20)$$

Considering boundary conditions (Eq. (16)), the temperature profile becomes:

$$\theta = \frac{1}{T_0\ln(h)}\times\left[(T_i - T_o)\ln\zeta + T_o\times\ln h\right] \quad (21)$$

Substituting Eq (21) in Eq (15) yields the displacement u0 as follows:

$$f(\zeta) = (\frac{\partial\Lambda_r}{\partial\zeta}\theta + \Lambda_r\frac{\partial\theta}{\partial\zeta}) \quad (22)$$

$$\frac{\partial}{\partial\zeta}\left[\frac{1}{\zeta}\frac{\partial}{\partial\zeta}(\zeta u_0)\right] = f(\zeta) \quad (23)$$

$$u_0(\zeta) = C_1 + C_2\zeta^{-1} + \zeta^{-1}\int_0^{\zeta}\zeta\left[\int_0^{\zeta}f(\zeta)d\zeta\right]d\zeta \quad (24)$$

Stress distribution in various directions may be obtained by substituting Eq. (24) into Eqs. (9) and (10).

3. Numerical results and discussion

In this section, plots corresponding to distribution of displacement and stresses are discussed. Fig. 4 illustrate dimensionless displacement across thickness of the cylinder for different layouts at aspect ratios ($h=\frac{r_i}{r_o}$) of 0.2, 0.4, and 0.6, 0.8 in Fig.4a and Fig.4b, respectively.

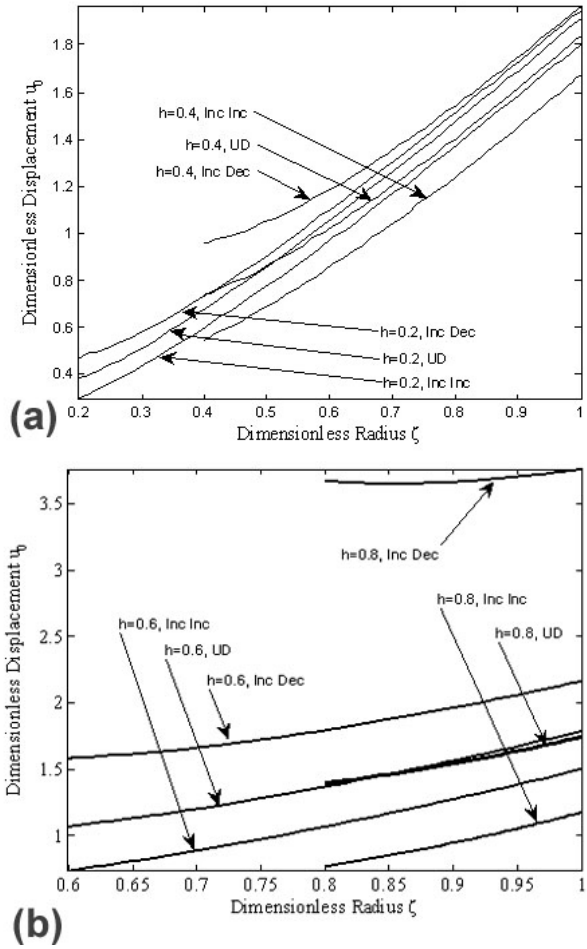

Fig. 4. Distribution of dimensionless displacement, u_0, versus dimensionless radius, ζ, of CNT for different layouts at aspect ratios of a) 0.2, 0.4 and b) 0.6, 0.8 (T_i=300K, T_o=500K and V_{CN}=0.11).

Larger aspect ratio corresponds to smaller and thinner cylinders. As can be seen, dimensionless displacement changes almost linearly with dimensionless radius and the rate of this change is less for higher aspect ratios h. Also, maximum displacement takes place at the outer surface of cylinder and for all aspect ratios considered here, Inc-Inc layout shows the least displacement, compared with Inc-Dec and UD. The difference between Inc-Inc and Inc-Dec for the same h becomes more apparent for higher aspect ratios. As far as bonding between CNT and the matrix is concerned, for constant volume fraction of CNT which is the case in this study, as h is increased, displacement and consequently interface debonding between matrix and CNT are increased.

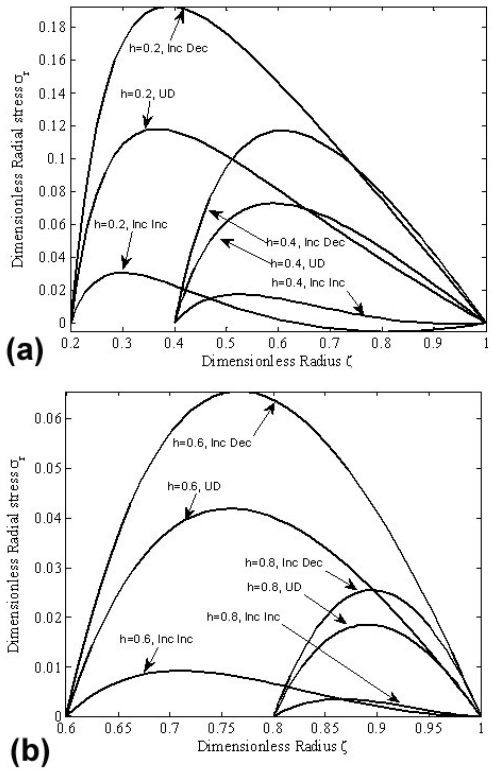

Fig.5. Distribution of dimensionless radial stress, σr, versus dimensionless radius, ζ, of CNT for various layouts and aspect ratios of a) 0.2, 0.4 and b) 0.6, 0.8 (Ti=300K, To=500K and VCN = 0.11).

Figures 5 show distribution of dimensionless radial stress across thickness of the cylinder for various layouts and aspect ratios as above. As can be seen, maximum stress takes place near the inner surface of the cylinder for low h and decreases with increasing h. For all aspect ratios considered here, Inc-Inc layout shows the least dimensionless radial stress, compared with Inc-Dec and UD.

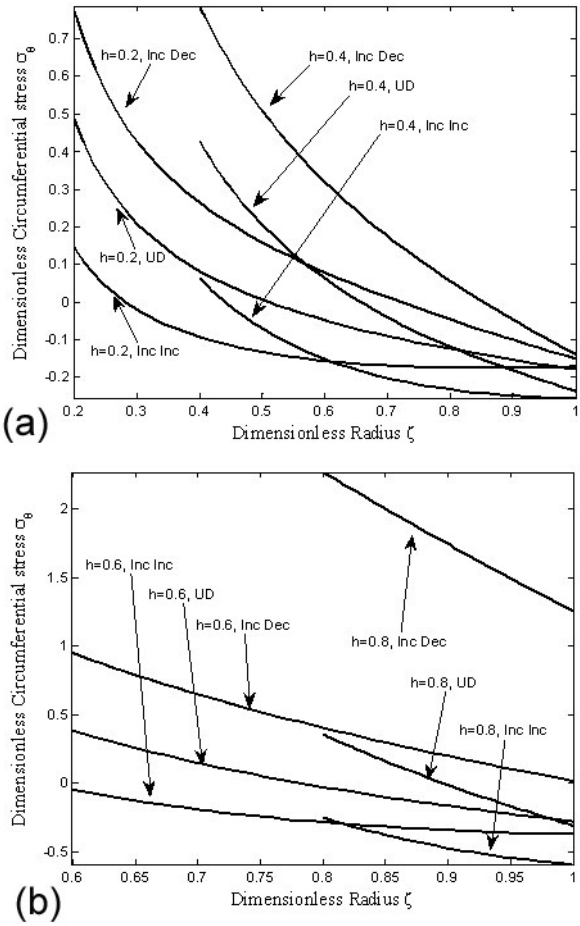

Fig.6. Distribution of dimensionless circumferential stress, σθ, versus dimensionless radius, ζ, of CNT for different layouts at aspect ratios of a) 0.2, 0.4 and b) 0.6, 0.8 (Ti=300K, To=500K and VCN=0.11).

Figures 6 depict distribution of dimensionless circumferential stress across thickness of the cylinder for various layouts and aspect ratios. Maximum tensional circumferential stress takes

place at the inner surface of the cylinder. Circumferential stress increases with increasing h irrespective of the layout type. The same as radial stress in Figures 5, for all aspect ratios, Inc-Inc layout shows the least dimensionless circumferential stress, compared with Inc-Dec and UD.

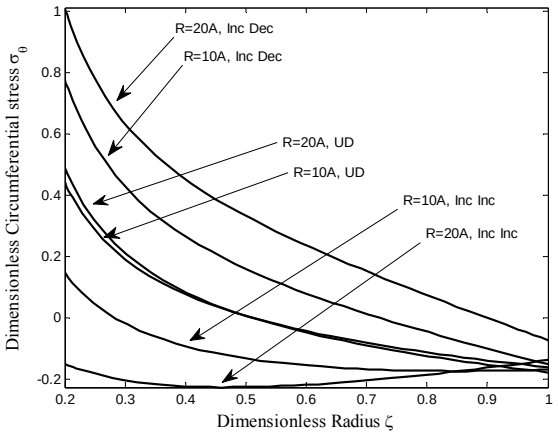

Fig.7. Distribution of dimensionless circumferential stress, σr, versus dimensionless radius, ζ, of CNT for two radius of SWCNTs (R = 10A0, 20 A0) (Ti = 300K, To = 500K , VCN = 0.11 and h = 0.2).

Fig. 7 show circumferential stress distribution across thickness of the cylinder in h = 0.2 for two radius of SWCNTs. It is observed from this figure that when radius of CNTs is increased, the circumferential stress in Inc-Dec layout increases; while for Inc-Inc, the riverse is true. Also, increasing radius of CNTs, doesn't seem to affect significantly dimensionless circumferential stress in UD layout. Circumferential stress decreases with increasing ζ for all radii and layouts of CNTs.

Figure 8 shows the distribution of Von-Mises stress across thickness of the cylinder in h = 0.4 for various layouts. The plots of axial stresses, σz, versus the dimensionless radius have not been presented here for brevity.

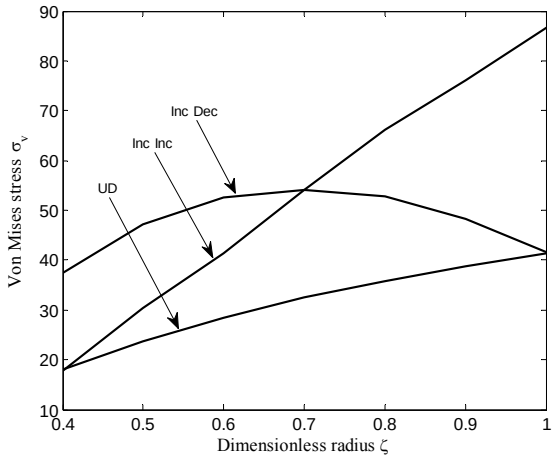

Fig.8. Distribution of dimensionless Von-Mises stress, σv, versus dimensionless radius, ζ, of CNT for various layouts (Ti=300K, To = 500K , VCN = 0.11 and h = 0.4).

As can be seen, the Von-Mises stress has increased almost linearly with the dimensionless radius for both cases of Inc Inc and UD layouts with the former having a higher gradient. Also, minimum Von-Mises stress happens for UD layout and it is therefore, recommended for the optimum design of nanocomposite thick-walled cylindrical vessels.

4. Conclusion remarks

Stresses and displacement analysis of a thick-walled nanocomposite cylinder reinforced by functionally graded (FG) single-walled carbon nanotubes (SWCNTs) in radial direction has been presented while subjected to a steady state thermal field. The SWCNTs are assumed aligned, straight with infinite length and a uniform layout. Two types of variations in the volume fraction of SWCNTs were considered in the structure of the FG cylinder along the radius from inner to outer surface, namely: incrementally increasing (Inc Inc) and incrementally decreasing (Inc Dec). These are

compared with uniformly distributed (UD) structure. Mori-Tanaka method is employed for stress-strain analysis. Using equations of motion, stress-strain and their corresponding constitutive correlations of a polystyrene vessel, a second order ordinary differential equation is proposed based on radial displacement. This is then solved in order to obtain the distribution of displacement and radial, circumferential and axial stresses. For constant temperatures at the inner and outer surfaces of the FG cylinder considered here, results in this work indicate that radial and circumferential stresses and displacement are lower for the Inc Inc FG cylinder, and the axial stresses are higher irrespective of the structure of the FG material. Furthermore, increasing the aspect ratios h, has reduced radial stress in all layouts. Circumferential stress for UD and Inc Inc cylinders and has increased it for Inc Dec cylinder. As far as variations of the SWCNTs radius is concerned, increasing this

a) has reduced radial and circumferential stresses in Inc Inc cylinder

b) has increased radial and circumferential stresses in Inc Dec cylinder

The corresponding analyses of axial sresses have not been presented here for brevity of results. However, results on Von Mises stress show that it has increased almost linearly with the dimensionless radius for both cases of Inc Inc and UD layouts. UD layout is recommended for optimum design of nanocomposite thick-walled cylindrical vessels as minimum Von-Mises stress takes place in it.

Nomenclature

σ	Stress
ε	Strain
T	Temperature
u	Displacement in radial directi
k, m, n, l, p	Hill's elastic moduli
E_m	Elastic moduli of matrix
R	Radius of carbon nanotube
c_r , c_m	Volume fractions of carbon nanotube and matrix, respectively
w_{CN}	Mass fraction of carbon nano
$\alpha_r^{CN}, \alpha_z^{CN}, \alpha^m$	Thermal expansion coeffici for carbon nanotube and matrix
$\alpha_r, \alpha_z, \alpha_\theta$	Thermal expansion coefficie a nanocomposite
ν_z^{CN} , ν^m	Poisson's ratio for carbon nanotube and matrix, respectively
ν_ζ	Poisson's ratio for a nanocomposite.
ρ_{CN}, ρ_m	Densities of carbon nanotu and matrix.
ζ	Dimensionless Radius
h	Dimensionless aspect ratio
$\lambda_r, \lambda_\theta, \lambda_z$	Thermal modulus of nanocomposite (in the subscript dirction)

References

[1] Saito R, DresselhausG, Dresselhaus M S. Physical Properties of Carbon Nanotubes. Imperial College Press: London; 1998.

[2] Qian D, Wagner G J, Liu W K, Yu M F and Ruoff R S. Mechanics of Carbon Nanotubes. Appl Mech Rev 2002; 55(6): 495–533.

[3] Ajayan PM, Stephan O, Colliex C, Trauth D. Aligned carbon nanotube arrays formed by cutting a polymer resin—nanotube composite. Science 1994; 256: 1212–4.

[4] Lourie O, Cox D M, Wagner H D. Buckling and Collapse of Embedded Carbon Nanotube. Phys Rev Lett 1998; 81(8): 1638–41.

[5] Haggenmueller R, Gommans H H, Rinzler A G, Fischer J E, Winey K I. Aligned Single-Wall Carbon Nanotubes In Composites by

Melt Processing Methods. Chem Phys Lett 2000; 330: 219–25.

[6] Fidelus J D, Wiesel E, Gojny F H, Schulte K,Wagner H D. Thermo-mechanical properties of randomly oriented Carbon/epoxy nanocomposites. Compos Part A: Appl Sci Manufact 2005; 36:1555–61.

[7] Bonnet P, Sireude D, Garnier B, Chauvet O. Thermal properties and percolation in carbon nanotube–polymer composites. J Appl Phys 2007; 91: 201910.

[8] Qian D, Dickey E C, Andrews R, Rantell T. Load Transferand and Deformation Mechanisms in Carbon Nanotube-Polystyrene Composites. Appl Phys Lett 2000; 76: 2868–70.

[9] Odegard GM, Gates T S, Wise K E, Park C, Siochi E J. Constitutive Modeling of Nanotube-Reinforced Polymer Composites. Compos Sci Technol 2002; 63(11): 1671–87.

[10] Wuite J, Adali S. Deflection and stress behaviour of nanocomposite reinforced beams using a multiscale analysis. Comps Struct 2005; 71:388–96.

[11] Vodenitcharova T, Zhang L C. Bending and local buckling of a nanocomposite beam reinforced by a single-walled carbon nanotube. Int J Solids Struct 2006; 43:3006–24.

[12] Han Y, Elliott J. Molecular dynamics simulations of the elastic properties of polymer/ carbon nanotube composites. Comput Mater Sci 2007; 39:315–23.

[13] Zhu R, Pan E, Roy AK. Molecular dynamics study of the stress–strain behavior of carbon-nanotube reinforced Epon 862 composites. Mater Sci Eng A 2007; 447: 51–7.

[14] Shen HS. Nonlinear bending of functionally graded carbon nanotubereinforced composite plates in thermal environments. Compos Struct 2009; 91:9–19.

[15] Ke L. L., Yang J., Kitipornchai S. Nonlinear free vibration of functionally graded carbon nanotube-reinforced composite beams. Compos Struct 2010; 92(3): 676-83.

[16] Wang X. Thermal shock in a hollow cylinder caused by rapid arbitrary heating. J Sound Vib 1995; 183: 899–906.

[17] Cho H, Kardomateas G A, Valle C S. Elastodynamic solution for the thermal shock stresses in an orthotropic thick cylindrical shell. J Appl Mech 1998; 65: 184–192.

[18] Ding H J, Wang H M, Chen W Q. A theoretical solution of cylindrically isotropic cylindrical tube for axisymmetric plane strain dynamic thermoelastic problem. Acta Mech Solida Sinica 2001; 14: 357–63.

[19] Pelletier J L, Vel S S. An exact solution for the steady-state thermoelastic response of functionally graded orthotropic cylindrical shells. Int J Solids Struct 2006; 43: 1131–58.

[20] Horgan C O, Chan A M. The pressurized hollow cylinder or disk problem for functionally graded isotropic linearly elastic materials. J Elasticity 1999; 55: 43–59.

[21] Tarn J Q. Exact solutions for functionally graded anisotropic cylinders subjected to thermal and mechanical loads. Int J Solids Struct 2001; 38: 8189–206.

[22] Abd-Alla A M, Farhan A M. Effect of the non-homogenity on the composite infinite cylinder of orthotropic material. Phys Lett A 2008; 372: 756–60.

[23] Shi D L, Feng X Q, Huang Y Y, Hwang K C, Gao H. The effect of nanotube waviness and agglomeration on the elastic property of carbon nanotube–reinforced composites. J Eng Mater Technol 2004; 126: 250-7.

[24]Hill R. A Self- Consistent Mechanics of Composite Materials J Mech Phys Solids 1965; 13: 213–22.

[25] Popov VN, Van Doren V E, Balkanski M. Elastic Properties of Crystals of Single-Walled Carbon Nanotubes. Solid State Commun 2000; 114: 395–9.

[26] Mark J E. Polymer data handbook, Oxford University Press, New York. Oxford: 828-37, 1999.

[27] Hetnarski R B, Eslami M R. Thermal stresses advanced theory and application. Solid Mechanics;2008.